NOAA Technical Memorandum ERL AOML-26

A SPLICED NUMERICAL GRID HAVING APPLICATIONS TO STORM SURGE

W. C. Thacker

Atlantic Oceanographic and Meteorological Laboratories
Miami, Florida
December 1976

noaa NATIONAL OCEANIC AND ATMOSPHERIC ADMINISTRATION / Environmental Research Laboratories

NOAA Technical Memorandum ERL AOML-26

A SPLICED NUMERICAL GRID HAVING APPLICATIONS TO STORM SURGE

W. C. Thacker
Sea-Air Interaction Laboratory

Atlantic Oceanographic and Meteorological Laboratories
Miami, Florida
December 1976

UNITED STATES
DEPARTMENT OF COMMERCE
Juanita M. Kreps, Secretary

NATIONAL OCEANIC AND
ATMOSPHERIC ADMINISTRATION
Robert M. White, Administrator

Environmental Research
Laboratories
Wilmot N. Hess, Director

DISCLAIMER

The Environmental Research Laboratories do not approve, recommend, or endorse any proprietary product or proprietary material mentioned in this publication. No reference shall be made to the Environmental Research Laboratories, or to this publication furnished by the Environmental Research Laboratories, in any advertising or sales promotion which would indicate or imply that the Environmental Research Laboratories approve, recommend, or endorse any proprietary product or proprietary material mentioned herein, or which has as its purpose an intent to cause directly or indirectly the advertised product to be used or purchased because of this Environmental Research Laboratories publication.

CONTENTS

A Spliced Numerical Grid Having Applications to Storm Surge

W. C. Thacker

ABSTRACT

A spliced numerical grid, such as might be used to calculate storm surges simultaneously within bays and along the open coast, is used to obtain solutions to the shallow water wave equations. Spurious, numerically induced flow is generated at the splice, but the amplitude of this noise is small so long as there are no variations of the solution on the scale of the grid spacings. Analytical solutions are obtained for a two-depth basin, and the agreement with numerical solutions is excellent for both trapped waves and seiche waves. Such a spliced grid with the finer portion in shallow water has advantages over a uniform grid in that it resolves the waves better over the entire basin and in that the time step can be larger for the same resolution in shallow water.

1. INTRODUCTION

Work on a spliced grid has been motivated by the need for mathematical models capable of predicting hurricane storm surges in bays and estuaries. The National Weather Service is using the SPLASH models of Jelesnianski (1970) to predict surges along the open coast. These models have a grid spacing of 4 nmi, which is sufficient to resolve the hurricane and the flow on the continental shelf but is too large to resolve the flow within bays and estuaries. Other models (Overland, 1975; Reid and Bodine, 1968) with smaller grid spacing have been used to calculate the surge within bays. They require the results of a model such as SPLASH to provide seaward boundary conditions for bay calculations. Since there is strong

coupling between the bay and the shelf regions, it is necessary to use a model that is appropriate to both regions.

One possibility is to use a fine grid, appropriate for the bay, throughout the extended region consisting of both the bay and the shelf. However, this is undesirable for two reasons. First, more computations than necessary must be made in the shelf region in each time step because of the excess number of grid points there. More importantly, because the maximum size of the time step is inversely proportional to the square root of the greatest depth, an undesirably large number of time steps is needed.

Another possibility is to use a fine computational grid for the bay spliced to a coarse grid for the shelf. This avoids an excess of computations in the shelf region and allows for a larger time step.

As a test of such a spliced grid, normal modes of a square basin were computed and compared with analytic solutions. In particular, the important case corresponding to shallow water with a fine grid and deep water with a coarse grid was considered. Agreement between numerical and analytic solutions for both the trapped waves (edge waves) and the seiche waves was excellent.

2. ANALYTIC SOLUTION FOR A TWO-DEPTH BASIN

Storm surge calculations are based on the shallow water wave equations,

$$\left.\begin{aligned} \frac{\partial U}{\partial t} + gD\,\frac{\partial H}{\partial x} &= 0 \\ \frac{\partial V}{\partial t} + gD\,\frac{\partial H}{\partial y} &= 0 \\ \frac{\partial H}{\partial t} + \frac{\partial U}{\partial x} + \frac{\partial V}{\partial y} &= 0 \end{aligned}\right\}, \qquad (1)$$

where U and V are the x- and y-components of transport, H is the elevation of water above mean sea level, D is the depth of the basin, and g is the acceleration of gravity. These equations are solved for the variable depth basin, illustrated in

Figure 1, having depths D_1 for $0<x<L/2$ and D_2 for $-L/2<x<0$. The boundary conditions are $U=0$ for $x=\pm L/2$, and $V=0$ for $y=0$ and $y=L$. At $x=0$, U and H must be continuous; the y-component of the velocity V/D, not the transport, must also be continuous.

In solving for the normal mode solutions, U_1, V_1, and H_1, which are solutions for the region with depth D_1 are matched to corresponding solutions U_2, V_2, and H_2, for the region with depth D_2. These solutions are given by

$$\left.\begin{aligned}
U_1&=\eta_1\left(\frac{gD_1k_1^2}{k_1^2+k_y^2}\right)^{\frac{1}{2}}\sin k_1(x-L/2)\cos k_y y\sin\omega t\\
V_1&=\eta_1\left(\frac{gD_1k_y^2}{k_1^2+k_y^2}\right)^{\frac{1}{2}}\cos k_1(x-L/2)\sin k_y y\sin\omega t\\
H_1&=\eta_1\cos k_1(x-L/2)\cos k_y y\cos\omega t\\
U_2&=\eta_2\left(\frac{gD_2k_2^2}{k_2^2+k_y^2}\right)^{\frac{1}{2}}\sin k_2(x+L/2)\cos k_y y\sin\omega t\\
V_2&=\eta_2\left(\frac{gD_2k_y^2}{k_2^2+k_y^2}\right)^{\frac{1}{2}}\cos k_2(x+L/2)\sin k_y y\sin\omega t\\
H_2&=\eta_2\cos k_2(x+L/2)\cos k_y y\cos\omega t
\end{aligned}\right\}\quad\cdot\quad(2)$$

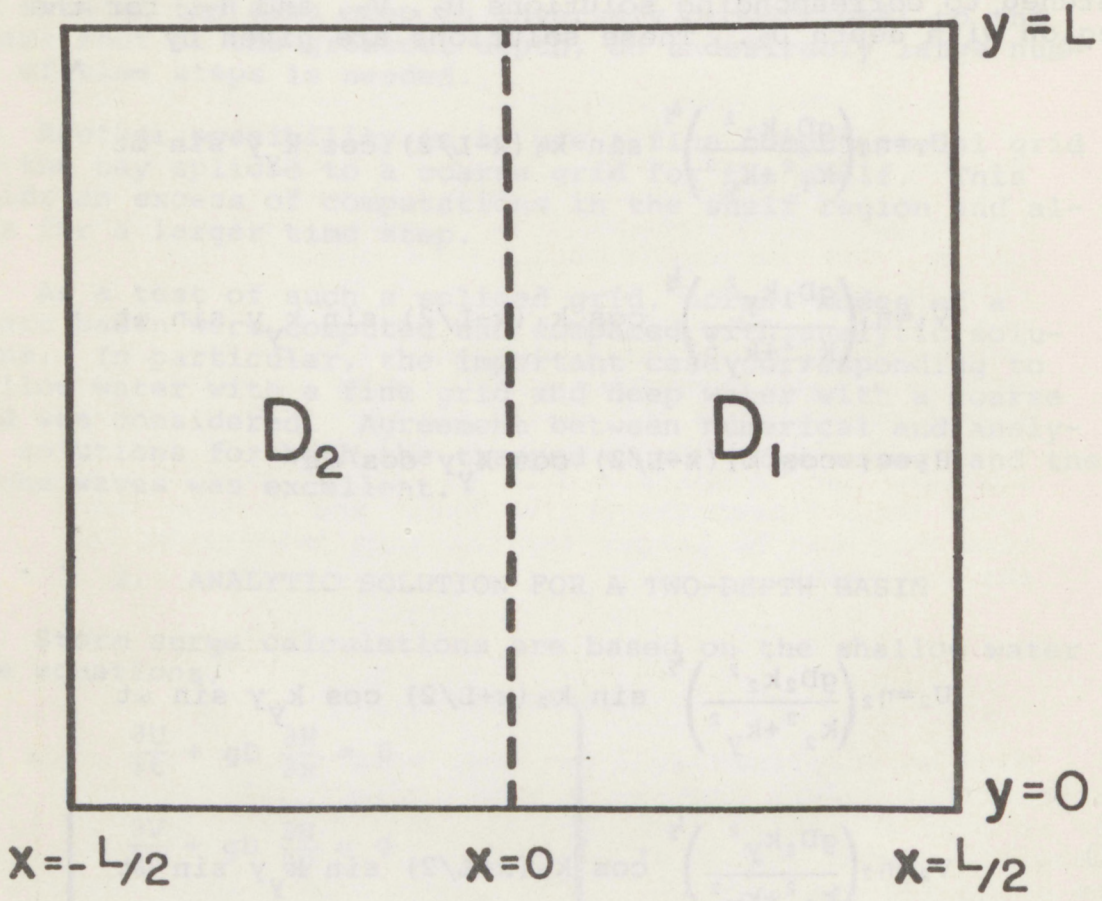

Figure 1. Variable depth basin.

To maintain continuity at $x=0$, ω and k_y must be the same for the two regions. The boundary conditions, $V_1=V_2=0$ at $y=0,L$, require that $k_y=\frac{n\pi}{L}$, where n is an integer. The wave numbers k_1 and k_2 must be determined by the continuity conditions at $x=0$,

$$\left.\begin{aligned} \eta_1 \cos\frac{k_1 L}{2} &= \eta_2 \cos\frac{k_2 L}{2} \\ -\eta_1 \, gD_1 \, k_1 \sin\frac{k_1 L}{2} &= \eta_2 \, gD_2 \, k_2 \sin\frac{k_2 L}{2} \end{aligned}\right\} \quad (3)$$

and by the dispersion equations,

$$\omega^2=gD_1(k_1^2+k_y^2)=gD_2(k_2^2+k_y^2). \quad (4)$$

The solutions for k_2 can be displayed graphically as the intersections of the curves $f=f_1(\theta)$ and $f=f_2(\theta)$, where

$$\left.\begin{aligned} f_1 &= -D_1\sqrt{\frac{D_2}{D_1}\theta^2-\left(\frac{D_1-D_2}{D_1}\right)\left(\frac{n\pi}{2}\right)^2}\,\tan\sqrt{\frac{D_2}{D_1}\theta^2-\left(\frac{D_1-D_2}{D_1}\right)\left(\frac{n\pi}{2}\right)^2} \\ f_2 &= D_2\,\theta\tan\theta \\ \theta &= \frac{k_2 L}{2} \end{aligned}\right\} . \quad (5)$$

A negative argument of the square root in the expression for f_1, corresponding to $k_1^2<0$, corresponds to waves trapped in the shallow regions of the basin. For those modes, the factors $\cos k_1(x-\frac{L}{2})$ and $\sin k_1(x-L/2)$ in (2) should be replaced

with $\cosh \ell_1(x-\frac{L}{2})$ and $\sinh \ell_1(x-L/2)$, where $\ell_1^2=-k_1^2<0$. Likewise in (3), $\cos \frac{k_1 L}{2}$ and $\sin \frac{k_1 L}{2}$ become $\cosh \frac{\ell_1 L}{2}$ and $-\sinh \frac{\ell_1 L}{2}$, and in (4), k_1^2 becomes $-\ell_1^2$. Then

$$f_1 = D_1\sqrt{\left(\frac{D_1-D_2}{D_1}\right)\left(\frac{n\pi}{2}\right)^2 - \frac{D_2}{D_1}\theta^2}\ \tanh\sqrt{\left(\frac{D_2-D_1}{D_1}\right)\left(\frac{n\pi}{2}\right)^2 - \frac{D_2}{D_1}\theta^2}\ . \quad (6)$$

Note that this is never the case for n=0, i.e., for motion that is uniform in the direction parallel to the interface; and further note that the modes with most variation in the direction parallel to the interface are most likely to be trapped in shallow water; the greater the difference in depth, the larger the number of trapped modes. Meyer (1971) has recently reviewed waves trapped by depth variations.

The graphical solutions for k_2 for a constant depth basin, $D_1=D_2$, are shown in Figure 2. These solutions are the same for all values of n since, for a constant depth basin, k_2 and k_1 are independent of k_y. The solutions are $k_2=k_1=\frac{m\pi}{L}$. Thus the normal modes can be identified by the two integers, m and n, corresponding to the x- and y-variations.

The corresponding solutions for the case $D_1=4D_2$ are shown in Figure 3. For unequal depths, k_2 and k_1 are no longer independent of k_y. The solutions of Figure 3 correspond to $k_y=\frac{\pi}{L}$ (n=1). Again, the x-variation can be identified by a non-negative integer, m, which can be chosen to be the same as that used in the limit $D_1 \to D_2$. The lowest mode, m=0, which corresponded to no x-variation when $D_1=D_2$, now has x-variation for $D_1=4D_2$ and is a trapped wave.

The solutions for the same case, $D_1=4D_2$, but for the next higher y-variations (n=2), are shown in Figure 4. Now the two modes, m=0 and m=1, are trapped waves.

Table 1 contains the values of k_2 and k_1 or ℓ_1 for modes with $n\leq 4$ and $m\leq 4$. For this case $D_1=4D_2$. These values were obtained by numerical solution of (5) and (6).

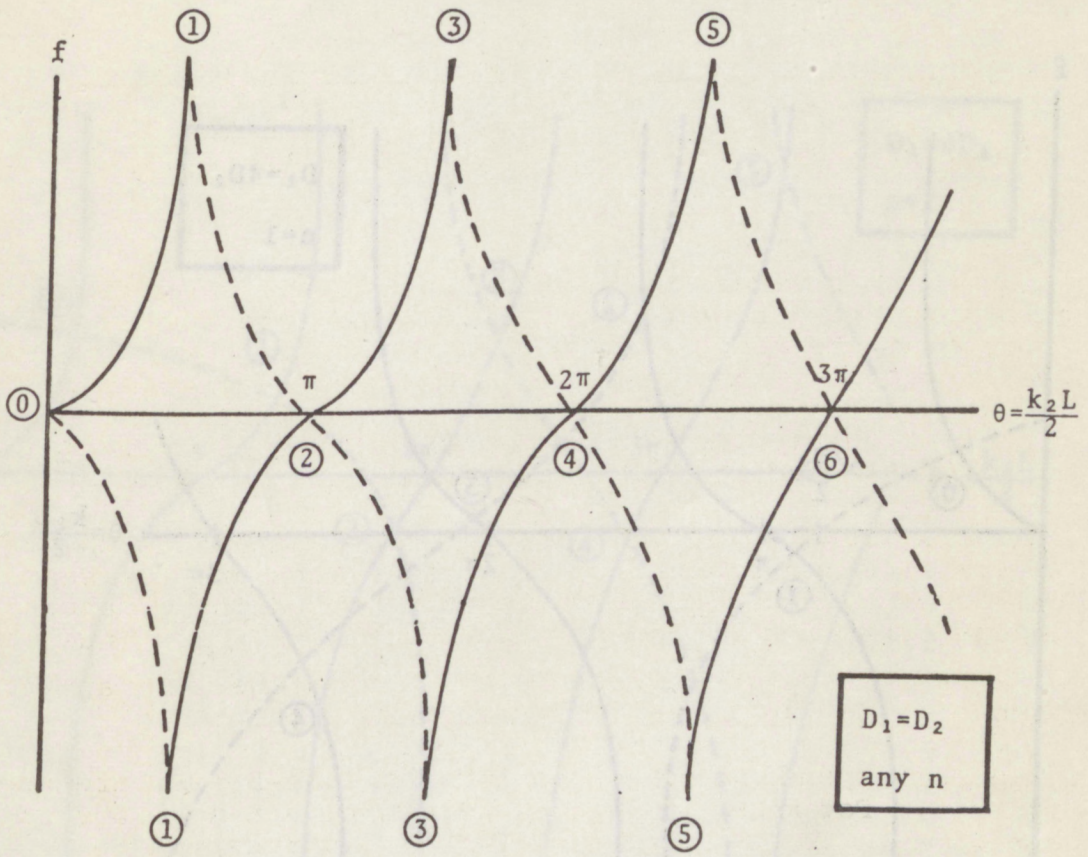

Figure 2. Solid curves represent f_2; dashed curves, f_1. Solutions for $k_2 = \frac{m\pi}{L}$ are represented by (m). For odd (m), the curves intersect at infinity.

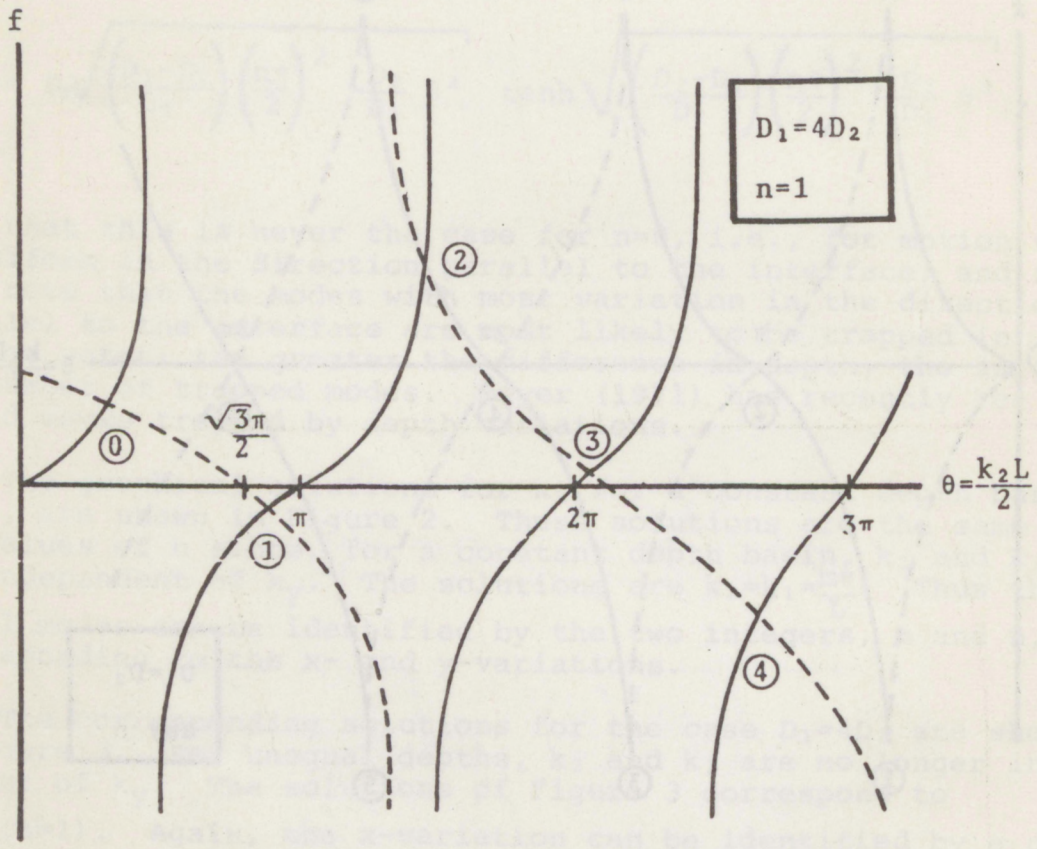

Figure 3. Solid curves represent f_2; dashed curves, f_1. The modes are labeled (m) to correspond to Figure 2. The zeroth mode is a trapped wave.

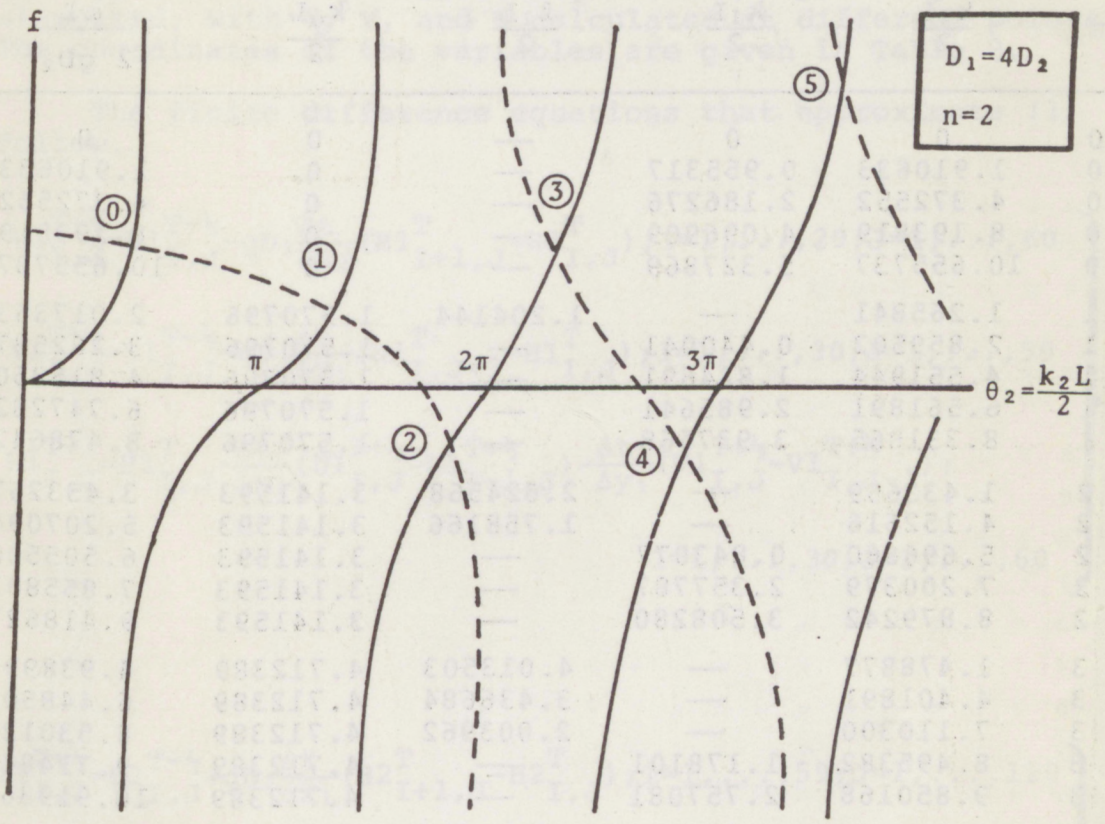

Figure 4. Intersection of solid curve (f_2) with the dashed curves (f_1) give the solutions for shallow-water wavenumber, k_2. Again, the modes are labeled (m) to correspond to Figure 2. Modes m=0 and m=1 are trapped waves.

Table 1. Values of wavenumbers and frequencies for normal modes of basin with $D_1=4D_2$. The integer, m, which indexes the x-variation corresponds to

$$k_1=k_2=\frac{m\pi}{L} \text{ if } D_1 \to D_2.$$

m	n	$\frac{k_2 L}{2}$	$\frac{k_1 L}{2}$	$\frac{\ell_1 L}{2}$	$\frac{k_y L}{2}$	$\frac{\omega L}{2\sqrt{gD_2}}$
0	0	0	0	—	0	0
1	0	1.910633	0.955317	—	0	1.910633
2	0	4.372552	2.186276	—	0	4.372552
3	0	8.193819	4.096909	—	0	8.193819
4	0	10.655737	5.327869	—	0	10.655737
0	1	1.265841	—	1.204144	1.570796	2.017363
1	1	2.859502	0.440041	—	1.570796	3.262537
2	1	4.551944	1.824691	—	1.570796	4.815350
3	1	6.561891	2.985641	—	1.570796	6.747282
4	1	8.331865	3.937568	—	1.570796	8.478642
0	2	1.433659	—	2.624568	3.141593	3.453257
1	2	4.152616	—	1.758166	3.141593	5.207094
2	2	5.696660	0.843077	—	3.141593	6.505500
3	2	7.200379	2.357787	—	3.141593	7.855893
4	2	8.879242	3.508280	—	3.141593	9.418627
0	3	1.478877	—	4.013503	4.712389	4.938997
1	3	4.401891	—	3.436684	4.712389	6.448508
2	3	7.110300	—	2.003962	4.712389	8.530122
3	3	8.495382	1.178101	—	4.712389	9.714841
4	3	9.850168	2.757081	—	4.712389	10.919360
0	4	1.501266	—	5.389375	6.283185	6.460048
1	4	4.489681	—	4.956764	6.283185	7.722412
2	4	7.417831	—	3.981553	6.283185	9.721246
3	4	10.088569	—	2.040590	6.283185	11.885186
4	4	11.2	1.435974	—	6.283185	12.890374

3. NUMERICAL SOLUTIONS USING A SPLICED GRID

The spliced grid used to calculate the normal modes of the two-depth basin is illustrated in Figure 5 for a simple case with very few grid points. Calculations were made with the grid spacing of $\Delta x_1=\Delta y_1=L/30$ in the deep region, and $\Delta x_2=\Delta y_2=L/60$ in the shallow region. The spliced grid is staggered, with U, V, and H calculated at different points. The coordinates of the variables are given in Table 2.

The finite difference equations that approximate (1) follow.

$$\left.\begin{aligned} Ul_{I,J}^{T+\frac{1}{2}} &= Ul_{I,J}^{T-\frac{1}{2}} - gD_1\frac{\Delta t}{\Delta x_1}\left(Hl_{I+1,J}^{T}-Hl_{I,J}^{T}\right);\ I=1,\ldots,29;J=1,\ldots,60 \\ Vl_{I,J}^{T+\frac{1}{2}} &= Vl_{I,J}^{T-\frac{1}{2}} - gD_1\frac{\Delta t}{\Delta y_1}\left(Hl_{I,J+1}^{T}-Hl_{I,J}^{T}\right);\ I=1,\ldots,30;J=1,\ldots,59 \\ Hl_{I,J}^{T+1} &= Hl_{I,J}^{T} - \frac{\Delta t}{\Delta x_1}\left(Ul_{I,J}^{T+\frac{1}{2}}-Ul_{I-1,J}^{T+\frac{1}{2}}\right) - \frac{\Delta t}{\Delta y_1}\left(Vl_{I,J}^{T+\frac{1}{2}}-Vl_{I,J-1}^{T+\frac{1}{2}}\right); \\ & \qquad I=1,\ldots,30;J=1,\ldots,60 \end{aligned}\right\},\quad (7a)$$

$$\left.\begin{aligned} U2_{I,J}^{T+\frac{1}{2}} &= U2_{I,J}^{T-\frac{1}{2}} + gD_2\frac{\Delta t}{\Delta x_1}\left(H2_{I+1,J}^{T}-H2_{I,J}^{T}\right);\ I=1,\ldots,59;J=1,\ldots,120 \\ V2_{I,J}^{T+\frac{1}{2}} &= V2_{I,J}^{T+\frac{1}{2}} - gD_2\frac{\Delta t}{\Delta y_1}\left(H2_{I,J+1}^{T}-H2_{I,J}^{T}\right);\ I=1,\ldots,60;J=1,\ldots,119 \\ H2_{I,J}^{T+\frac{1}{2}} &= H2_{I,J}^{T} + \frac{\Delta t}{\Delta x_1}\left(U2_{I,J}^{T+\frac{1}{2}}-U2_{I-1,J}^{T+\frac{1}{2}}\right) - \frac{\Delta t}{\Delta y_1}\left(V2_{I,J}^{T+\frac{1}{2}}-V2_{I,J-1}^{T+\frac{1}{2}}\right); \\ & \qquad I=1,\ldots,60;J=1,\ldots,120 \end{aligned}\right\},\quad (7b)$$

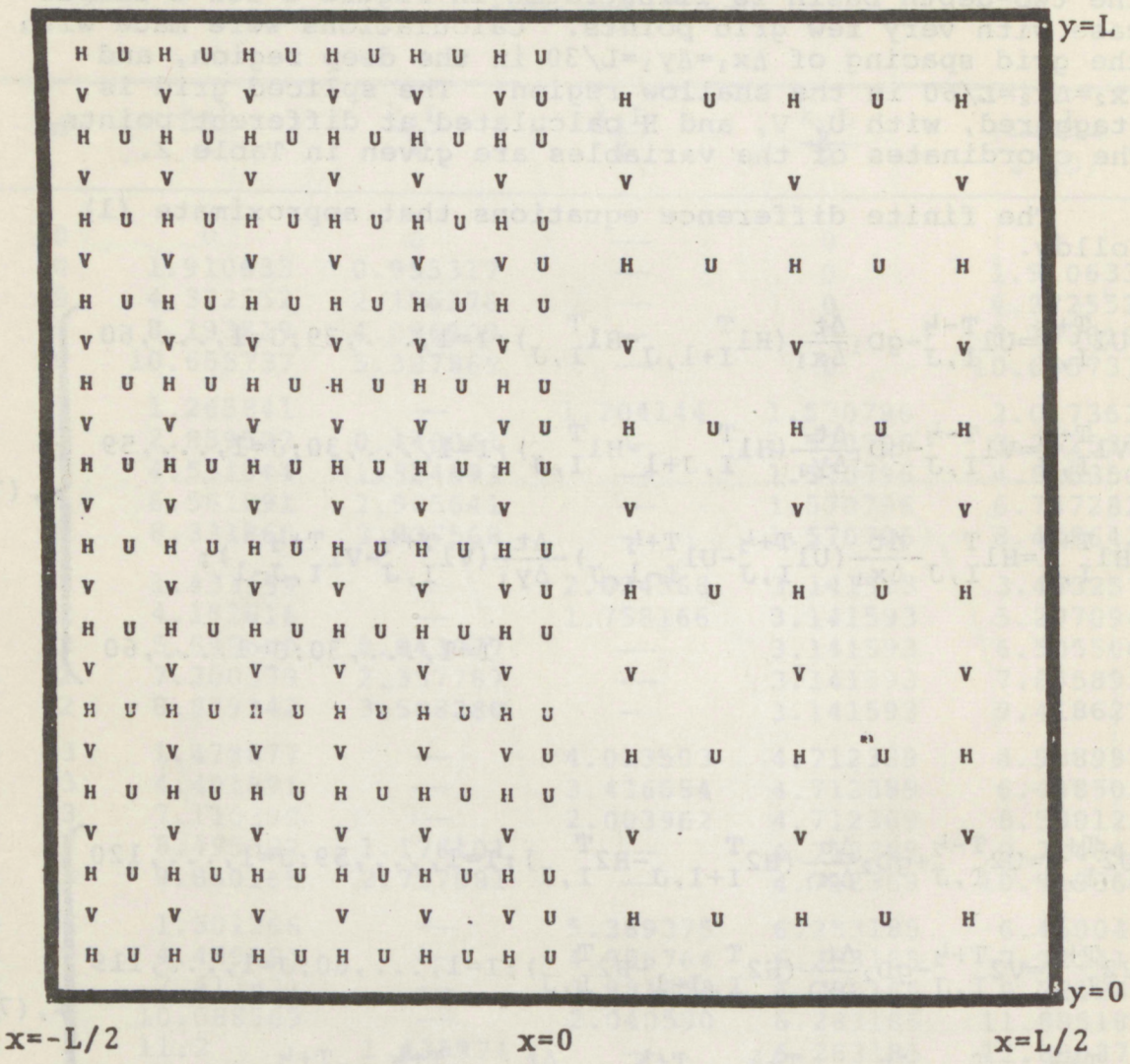

Figure 5. Numerical grid. The H, U, and V fields are staggered. The U field is evaluated along the splice.

Table 2. Coordinates of variables on spliced grid. Note that the variables U1(0,J) and U2(0,J) are situated on the splice. Further note that the x-coordinates for H1, U2, and V2 are negative for positive values of I.

Variable	x-coordinate	y-coordinate	Index Ranges
H1(I,J)	$\left(\frac{I-1/2}{60}\right)L$	$\left(\frac{J-1/2}{60}\right)L$	I=1,...,30;J=1,...,60
U1(I,J)	$\left(\frac{I}{60}\right)L$	$\left(\frac{J-1/2}{60}\right)L$	I=0,...,29;J=1,...,60
V1(I,J)	$\left(\frac{I-1/2}{60}\right)L$	$\left(\frac{J}{60}\right)L$	I=1,...,30;J=1,...,59
H2(I,J)	$-\left(\frac{I-1/2}{120}\right)L$	$\left(\frac{J-1/2}{120}\right)L$	I=1,...,60;J=1,...,120
U2(I,J)	$-\left(\frac{I}{120}\right)L$	$\left(\frac{J-1/2}{120}\right)L$	I=0,...,59;J=1,...,120
V2(I,J)	$\left(\frac{I-1/2}{120}\right)L$	$\left(\frac{J}{120}\right)L$	I=1,...,60;J=1,...,119

$$Ul_{0,J}^{T+\frac{1}{2}}=Ul_{0,J}^{T-\frac{1}{2}}-g(D_1+D_2)\frac{\Delta t}{\Delta x_1+\Delta x_2}(Hl_{1,J}^{T}-\frac{1}{2}(H2_{1,2J}^{T}+H2_{1,2J-1}^{T}));$$

$$J=1,\ldots,60$$

$$U2_{0,2J}^{T+\frac{1}{2}}=\frac{3}{4}Ul_{0,J}^{T+\frac{1}{2}}+\frac{1}{4}Ul_{0,J+1}^{T+\frac{1}{2}};J=1,\ldots,59$$

$$U2_{0,2J-1}^{T+\frac{1}{2}}=\frac{3}{4}Ul_{0,J}^{T+\frac{1}{2}}+\frac{1}{4}Ul_{0,J-1}^{T+\frac{1}{2}};J=2,\ldots,60$$

$$U2_{0,120}^{T+\frac{1}{2}}=\frac{5}{4}Ul_{0,60}^{T+\frac{1}{2}}-\frac{1}{4}Ul_{0,59}^{T+\frac{1}{2}}$$

$$U2_{0,1}^{T+\frac{1}{2}}=\frac{5}{4}Ul_{0,1}^{T+\frac{1}{2}}-\frac{1}{4}Ul_{0,2}^{T+\frac{1}{2}}$$

} ,(7c)

and

$$Ul_{M1,J}^{T+\frac{1}{2}}=0;J=1,\ldots,60;T=0,1,\ldots$$

$$U2_{M2,J}^{T+\frac{1}{2}}=0;J=1,\ldots,120;T=0,1,\ldots$$

$$Vl_{I,0}^{T+\frac{1}{2}}=Vl_{I,N1}^{T+\frac{1}{2}}=0;I=1,\ldots,30;T=0,1,\ldots$$

$$V2_{I,0}^{T+\frac{1}{2}}=V2_{I,N2}^{T+\frac{1}{2}}=0;I=1,\ldots,60;T=0,1,\ldots$$

} .(7d)

The superscripts refer to the time step, and the subscripts refer to the grid points. Equations (7a) and (7b) are very much alike. The notable difference is the sign of terms in (7b) involving Δx_2 differ from those in (7a) involving Δx_1. This is because the origin of the x-axis is taken at the splice, so I increases in the positive x-direction in (7a) and in the negative x-direction in (7b). Equations (7c) govern the perpendicu-

lar transports at the splice. Only the values appropriate to the coarse grid are evaluated from values at previous time steps. Values at points on the fine grid are obtained by interpolation and extrapolation. This is done in the spirit of the approximation involved in replacing derivatives with finite differences, i.e., a linear variation between grid points must be a good approximation. For completeness, the boundary conditions are given in equations (7d).

Numerical solutions for normal modes were obtained first for a basin of uniform depth, where $D_1=D_2$. The numerical solutions are good if the sinusoidal functions are well resolved on the coarse grid. Two cases are notable. The first corresponds to no variations in the solutions in the direction parallel to the splice, corresponding to $k_y=0$ in equations (3). For this case, V=0 both in the analytical solution and the numerical solution. The second case corresponds to no variations in the solutions in the direction perpendicular to the splice, corresponding to $k_x=0$ in (3). For this case, U=0 for all time in the analytical solution, but $U\neq 0$ in the numerical solution. This is due to the interpolation in (7c) necessary to join the two grids. The source of this noise in the U field is illustrated in Figure 6. The level of the noise can be controlled by controlling the number of grid points per wavelength, since linear interpolation involves the same approximation as replacing derivatives by finite differences. Although the noise is most apparent in the U field, there is also noise in the H and V fields that is less noticeable since it may be only one percent of the calculated value, rather than the entire value, which must be the case when comparing to U=0. Even the noise in the U field would not be apparent if only the first two digits of the numerical solutions were displayed. This noise due to interpolation might appear in any attempt to use a non-uniform grid. So long as there is little energy in the shortest wavelengths, this noise is not expected to be a problem.

The spliced grid shown in Figure 5 is ideally suited for the case $D_1=4D_2$ because it resolves the normal modes equally in the two regions. This can be seen from equation (4). The wavelengths in the two regions are given by $\lambda_1=2\pi/(k_y^2+k_1^2)^{\frac{1}{2}}$ or $\lambda_1=2\pi/(k_y^2-\ell_1^2)^{\frac{1}{2}}$ and $\lambda_2=2\pi/(k_y^2+k_2^2)^{\frac{1}{2}}$, so from (4), $\lambda_1=2\lambda_2$. Because the grid spacing is twice as large in region 1 as in region 2, the number of grid points per wavelength is given by

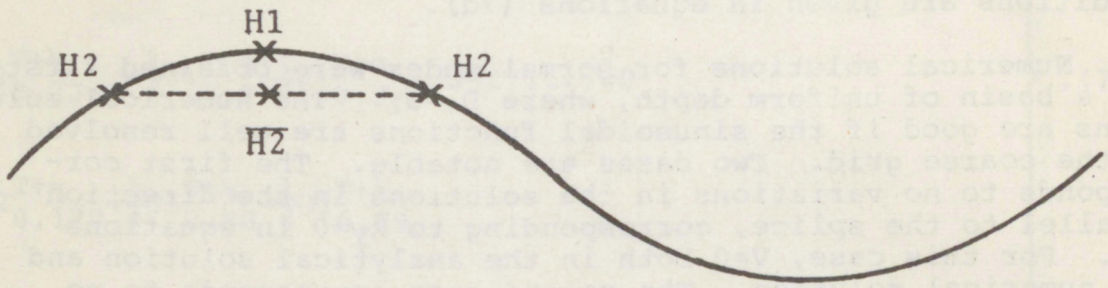

Figure 6. The sinusoid curve represents an H field along the splice. The value $\overline{H2}$ represents an interpolated value of the H2 field that should compare with the value H1 directly across the splice. Although there is no change in the elevation of the H field in the analytical solutions, there is an induced sloped across the splice due to the interpolation. It is this slope which leads to non-zero values of the U field in the numerical solution. When the finite difference approximation is good, linear interpolation is a good approximation, and the level of the noise in the U field is low.

$60\pi/(\omega L/2\sqrt{gD})$, which is greater than 10 for all of the modes listed in Table 1. Thus, all of these modes are fairly well resolved on the grid, and numerical results should be good to a few percent. The maximum time step determined by the stability conditions, $\Delta t=\Delta x_1/(2gD_1)^{\frac{1}{2}}$ and $t=\Delta x_2/(2gD_2)^{\frac{1}{2}}$, is the same for both regions of the grid. For a uniform grid, the time step would be determined by the deep region.

Table 3 compares the dimensionless frequencies, $\omega L/2\sqrt{gD}$ obtained by counting the number of sign changes of the height field at each computational point in one thousand time steps with the analytical results listed in Table 1. The frequencies were found to be the same at all grid points in both regions, except for modes with n=4. For those cases, the number of sign changes was not accurately counted in regions where the height field was essentially zero at all times. For most of the points, however, the frequency was found to be constant, even for n=4. The agreement shown in Table 2 is quite good, with differences between computed and analytical results of less than a few percent as expected from the resolution of the grid.

4. DISCUSSION

The excellent results of this test suggest that a similar spliced grid can be used in numerical models of storm surges for bays and estuaries. The principal restriction is that there be no wave components of the solutions that can be represented on the fine grid but not on the coarse grid. Since wave lengths increase from shallow to deep water, this restriction is not severe. Another way of stating this restriction is that the solutions must be sufficiently smooth that the interpolations necessary at the grid splice be a good approximation. But that is exactly the usual requirement that a finite difference must be a good approximation of a derivative for the numerical solution to be valid.

Table 3. A Comparison of values for $\omega L/2\sqrt{gD}$ obtained numerically and analytically for normal modes (m,n)

Mode		Dimensionless Frequency	
m	n	Computed	Analytical
1	0	1.87	1.91
2	0	4.40	4.37
3	0	8.13	8.19
4	0	10.66	10.66
0	1	2.00	2.02
1	1	3.20	3.26
2	1	4.80	4.82
3	1	6.80	6.75
4	1	8.53	8.48
0	2	3.47	3.45
1	2	5.27	5.21
2	2	6.63	6.51
3	2	7.97	7.86
4	2	9.60	9.42
0	3	5.00	4.94
1	3	6.49	6.45
2	3	8.55	8.53
3	3	9.86	9.71
4	3	11.11	10.92
0	4	6.42	6.46
1	4	7.73	7.72
2	4	9.73	9.72
3	4	11.90	11.89
4	4	12.83	12.89

5. REFERENCES

Jelesnianski, Chester P. (1970): "Bottom stress time-history" in linearized equations of motion for storm surges. Mon. Weather Rev., 98:462.

Meyer, R. E. (1971): Resonances of unbounded water bodies. Mathematical Problems in the Geophysical Sciences, 1. Geophysical Fluid Dynamics, pp. 181-227. William H. Reid, Editor, American Mathematical Society.

Overland, James E. (1975): Estimation of hurricane storm surge in Apalachicola Bay, Florida. NOAA Tech. Rept. NWS 17.

Reid, Robert O., and Bernie R. Bodine (1968): Numerical model for storm surges in Galveston Bay. J. Waterways and Harbors Div., Proc. American Society of Civil Engineers, 94:33.